Complex interaction between CMT equipment and robot controllers during the WAAM process: consequences for toolpath accuracy

Ricardo da Silva Viola, Xavier Balandraud, Fabien Poulhaon, Pierre Michaud, Emmanuel Duc

Complex interaction between CMT equipment and robot controllers during the WAAM process: consequences for toolpath accuracy

Ricardo Da Silva Viola[1,2], Xavier Balandraud[2], Fabien Poulhaon[1], Pierre Michaud[1], Emmanuel Duc[2,*]

[1] Univ. Bordeaux, ESTIA Institute of Technology, F-64210 Bidart, France

[2] Clermont Auvergne INP, Université Clermont Auvergne, CNRS, Institut Pascal, 63000 Clermont-Ferrand, France

[*]Corresponding author. Tel.: +33 (0)473288096. E-mail address: emmanuel.duc@sigma-clermont.fr

Abstract:

The WAAM additive manufacturing process is considered one of the most efficient and productive processes. Its implementation is based on the use of a Cold Metal Transfert (CMT) device by a robot. The geometrical quality and the mechanical behaviour of the manufactured parts depend on the uniformity of the material deposition rate and the uniformity of the energy input, throughout the realization of the part. This paper discusses the interactions between the CMT device and the robot during the manufacturing process. The reaction times between the two systems are not the same and depending on a specific parameterization, the real trajectory is disturbed by the start or stop of the electric arc. An experimental study on 8 trajectories and 3 parameters allows us to analyze the behavior of the robot, the accuracy of the trajectory and the acceleration and deceleration phases. As a general conclusion, compromises must be found in terms of continuous/discontinuous deposition and deposition outside the nominal deposition area or not. Based on the tests performed in this study, the semi-circular strategy appears to be the most relevant in the case of continuous deposition over the whole toolpath. Finally, a model has been proposed to compute the manufacturing time of any area of the layer based on a preliminary identification for a single area.

Keyword: Wire arc additive manufacturing; Path planning; Trajectory; Discontinuous deposition; Controller

1. Introduction

Wire arc additive manufacturing (WAAM) is a production process suitable for medium to large parts in the aeronautics field [1-4]. This process is characterized by high metal deposition capacity and reduced material waste, part cost and iteration time compared with standard processes [2-4]. The method consists of depositing molten metal through an electric arc between the nozzle and the already-deposited material in a sequence of two-dimensional (2D) layers using a robot to perform the movements [5]. The quality of the weld bead depends on various parameters, such as the quality of the wire, the wire feed speed (WFS), the travel speed (TS) and the heat input [1]. Weld bead geometry is controlled by optimizing the values of the deposition parameters [1, 6]. Models can also be used to simulate the solidification process of the metal [7]. To limit high residual stresses, internal defects, porosities and lack of fusion between adjacent weld beads, it is possible to control the deposition parameters or tilt the nozzle along the trajectory [8-10]. The mechanical quality of the final part depends on the combination of all the manufacturing input parameters [5].

In the case of a robotized process, the robot's kinematic behavior along the trajectory (previously programmed to build the part) is a determining factor [11]. In particular, slowing down the robot at constant WFS can lead to too much material being added locally: the layer is no longer regular [12, 13]. It has been established that the quality of the metal deposited is directly related to the strategy used, which makes toolpath planning of paramount interest for the WAAM process [6, 14]. An adequate toolpath is essential to ensure that the geometry of the deposit is close to or greater than the theoretical volume to be built [15]. The literature refers to various types of strategies, such as raster-pass, zigzag, contour or spiral in relation to material health, mechanical properties (such as strength and hardness) and geometric quality (shrinkage and warpage) [15-20]. The control of the volume of material deposited is also of great importance [21]. The most commonly-used strategies to achieve a constant deposition thickness are based on equidistant path generation methods [17, 19]. Toolpath planning is crucial and should be focused on the accuracy of the robot's movements in order to have a direct impact on the geometrical, material and mechanical qualities of the built part [10, 20-24].

Aldadur et al. studies the influence of different parameters and deposition strategies on the metallurgical quality of the manufactured parts [21]. The author insists on the fundamental character of the heat input and proposes a strategy that is recognized as more productive. Liu et al. applies classical robotics methods to a multi-head welding robot to calculate trajectories

in the task space and in the joint space [22]. Jin et al. develops an original process planning for the manufacturing of medical parts [23]. The author focuses on the whole process, including the filling of the layers, without addressing the kinematic behavior of the robot. Rauch et al. optimizes the strategy for the application case of aeronautical structural parts [24]. The influence of this strategy on the porosity, microstructure, microhardness and mechanical properties of the structure was studied. Srivastava et al. presents an extensive literature review on the WAAM process [25]. The author analyzes the influence of the different process parameters on the quality of the manufactured parts, in particular the deposit strategy. But it should be noted that the author considers that the robot behavior is perfect and does not influence the quality of the material deposit. Lim et al. enhances the approach by coupling additive manufacturing and machining, in a hybrid cell [26]. The hybrid cell allows to machine the layers during the manufacturing process, which improves the geometrical quality and the mechanical strength of the parts. This work focuses on a simple rectangular shape, and the influence of the kinematic behavior of the robot is not studied.

Comments can be made about the continuous/discontinuous character of the deposition:

- When the geometry of the 2D layer allows it, metal deposition is preferably composed of several straight sections without intermediate stops or restarts [27]. This procedure, widely used in toolpath programming, allows the continuity of the arc, avoiding stops that usually create defects [28]. Curved sections are often broken down into linear segments when the toolpath is computed [11]. Continuous deposition may have some disadvantages due to the high heat input [29]; the latter impacts the weld bead size and by consequence the geometry of the material deposit [30]. In practice, the higher the heat input, the higher the roughness of the part (due to a higher fluidity of the meltpool and spreading of the drop) and consequently the higher the costs associated with post-processing [11, 27, 29].
- For discontinuous deposition, a specific command (which is named *arc ON/OFF* for the KRC2 controller of the robot used in this study [32]) enables us to start (*arc ON*) and stop (*arc OFF*) metal deposition in specific sections of the toolpath. For example, the raster-pass strategy consists of depositing the metal along straight parallel sections in the same direction (deposition being stopped between these sections). Stops and restarts are inevitable for the production of all kinds of parts, as for most rib-web structures such as flaps, wing ribs, stiffeners or landing gear ribs in aircraft and aerospace parts [2, 3, 26]. Since these structures cannot be created with Eulerian paths, it is impossible to produce them through continuous deposition [33]. Discontinuous

depositions may lead to specific problems, such as longer deposition times, local defects and material accumulation, but they are unavoidable for many part geometries [17]. It should be noted that WAAM robotic systems offer such a feature, which is necessary to stop the wire feed. In general, the robot controller manages the cold metal transfer (CMT) equipment through a sequence of commands including the deposition parameters (*e.g. arc ON*/*OFF*). The real-time processing of this sequential action and the management of the wire feed can induce randomness in the regularity of the weld bead deposit.

Thus the literature shows that the use of WAAM processes necessarily imposes the precise control of the material input throughout the process [20]. For this, it is necessary to study the kinematic behavior of the robot, which generates the variations in speed and position of the end effector. Indeed, the realization of the task requires the best synchronization between the material input and the movement of the end effector. But two phenomena disturb this process: the evolution of the end effector feed rate due to the kinematic behavior of the robot axes and the launches or stops in material or energy supply that are not directly processed by the robot control, but by the added CMT system. The performance of the process is completely linked to the interaction between the robot and the CMT equipment. The problem can be generalized to the robotization of manufacturing processes relying on a precise tracking of the trajectory and implementing a manufacturing process. However, the behavior is specific to this robot and to the CMT equipment. Thus, whatever the technology used, it seems to us that this problem must be systematically addressed.

The Figure 1 shows the production of a WAAM part with several horizontal and vertical layers. The process requires perfect synchronization between robot movement, wire feed and energy supply. The first horizontal layer is obtained by several passes in a given direction. At the end of a pass, it must be selected whether or not to interrupt the wire feed (and therefore the energy input) before starting the next pass. In addition, at the end of a layer, the robot may have to wait to let the part cool down sufficiently to prevent it from collapsing in on itself. Controlling the robot's kinematic behavior and synchronizing it with the wire feed and energy supply are therefore critical to the quality of the manufactured part.

Fig. 1 Example of a part, obtained by WAAM process

In the present study, the movement of the nozzle to create of a rectangular layer was experimentally analyzed without physically depositing material (trajectory performance only). Different strategies, nozzle speeds and layer areas were compared in terms of deposition time, toolpath length and volume of "deposited" material. The consequences of discontinuous deposition (switching between *arc ON* and *arc OFF*) were also studied. The originality of this study is to better understand the complex interaction between CMT equipment and robot controllers. In fact, the performance of the process is directly linked to the interaction between CMT welding and the robot and the set of robot parameters. Several parameters allow to modify the kinematic behavior of the robot, like the speed or the accuracy, but the robot does not precisely manage the behavior of CMT.

Another objective is to propose a model to calculate the manufacturing time of any layer area from a preliminary identification for a single area.

The paper is organized as follows. Section 2 presents the experimental method used. Section 3 is dedicated to two preliminary studies on simple cases: impact of switching between *arc* ON and *arc OFF* during a linear trajectory at constant nominal speed; impact of a change in direction in the programmed nozzle movement. Section 4 presents and compares the results of the experimental test campaign. Finally, a manufacturing time estimation model is proposed in Section 5.

2. Experimental method

A test campaign was defined to compare different strategies and analyze various output parameters such as trajectory error and duration of acceleration/deceleration phases, as well as the impact of switching between *arc ON* and *arc OFF* (reproducing a discontinuous deposition).

2.1 Device

Figure 2 shows some images of the experimental device. A six-axis KUKA robot (KR 100-2 HA 2000 model) and a KRC2 controller were used to control the movement of the nozzle of a CMT device (Fronius). The spatial configuration of the robot allowed free and unobstructed movement of the equipment within the inert chamber that defines the robot's workspace. The latter was such that no kinematic singularity was possible. Most of the results in this study were obtained at a nozzle altitude z = 50 mm from the platform, in the middle of the chamber. However, other locations in the chamber were also considered for comparison purposes; see Section 4.4.

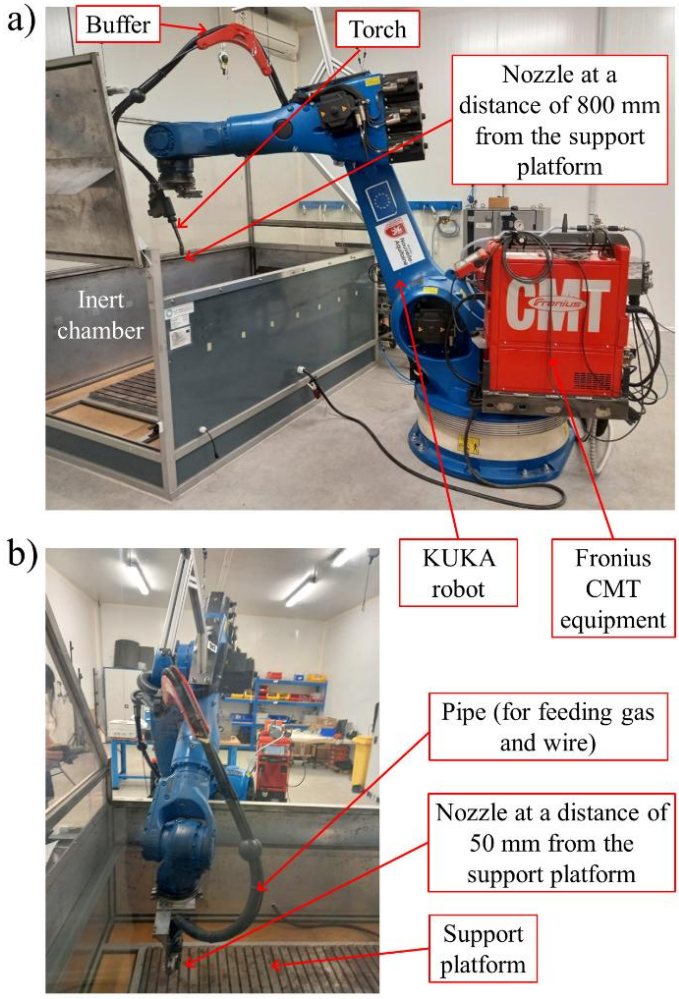

Fig. 2 Photos of the system. In the framework of this study, the nozzle movement was studied without activating the torch (trajectory definition only)

2.2 Strategies considered

Figure 3 presents the 8 strategies considered in the study: raster-pass, semi-circular, spiral, rectangular, swiping, as well as three triangular strategies differing in the angle of the triangles (45°, 60° and 90°). The blue lines represent the theoretical toolpaths of the nozzle, while the arrows indicate the travel direction. The green lines delimit a rectangular area to be theoretically filled by material deposit. This rectangle is named "*objective rectangle*" (OR) throughout the manuscript. We assumed a constant wire feed rate of 94.25 mm^3/s to calculate the volume of deposited material. This value was defined by previous experiments, not reported here; we performed a physical deposition (namely 2209 stainless steel) with the same equipment, with a WFS of 83.34 mm/s and a wire diameter of 1.2 mm. It can be noted that the semi-circular and the triangular strategies included sections of toolpath outside the OR, for

which the relevance of *arc OFF* is discussed in the present study. The spiral and rectangular strategies correspond to toolpaths remaining inside the OR, requiring thus *arc ON* over the whole toolpath. Finally, the raster-pass strategy also leads to a toolpath inside the OR, but alternating *arc ON* and *arc OFF*.

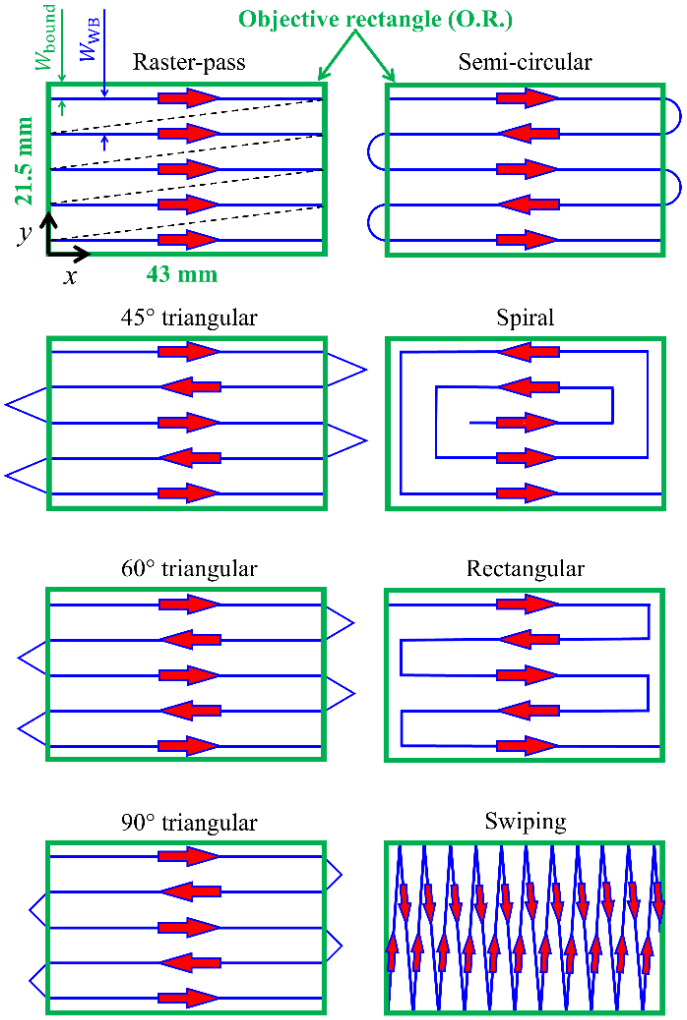

Fig. 3 Different strategies considered in the study

Two nominal travel speeds were considered in the study: 10 mm/s and 40 mm/s. The former value corresponds to the usual value used for our experiments on 2209 stainless steel. Two OR areas were considered: 21.5×43 mm^2 and 43×86 mm^2, sometimes referred to as "small OR" and "large OR" respectively in the following text for simplicity. It can be noted that the ratio between speeds and the ratio between areas were chosen to be the same (namely 4) for comparison purposes. The distance W_{WB} between the linear sections of adjacent parallel weld beads (see Fig. 2) was set to 4.43 mm. This value was previously defined by experiments on

2209 stainless steel. The number of horizontal weld beads n_{WB} was then defined from the ratio between W_{WB} and the width W of the OR:

$$n_{\mathrm{WB}} = \mathrm{floor}\left(\frac{W}{W_{\mathrm{WB}}}\right) \quad (1)$$

where $\mathrm{floor}(x)$ means the nearest integer lower than x. The remaining distance W_{bound} between the OR boundary and external depositions (see Fig. 2) can be then simply obtained by:

$$W_{\mathrm{bound}} = \frac{W - (n_{\mathrm{WB}} - 1) \times W_{\mathrm{WB}}}{2} \quad (2)$$

In fact, Equations (1) and (2) were considered to be valid if $W_{\mathrm{bound}} \leq 0.4\, W_{\mathrm{WB}}$ in order to deposit enough material at the boundary of the OR. If the inequality is not verified, n_{WB} must be increased by one: $n_{\mathrm{WB}} \leftarrow n_{\mathrm{WB}} + 1$. The numerical application gives n_{wb} equal to 5 and 10 for the small and large OR, respectively, and W_{bound} equal to 1.89 mm and 1.57 mm, respectively. Note that the choice of the areas for the OR comes from fabrication tests, not reported here. The value chosen for W_{WB} ensures a layer of material without porosity. The choice of W_{bound} ensures a sufficiently flat layer deposited over the OR, with the excess material (outside the RO) being machined away later.

Note that the values have been chosen to stress the robot in conditions compatible with real manufacturing. In the case of this study, the actual removal of material is not necessary to analyze the behavior of the system.

The tool path is calculated by a specific CAM system. This one only allows to specify the number of points on the path. Thus, the number of points is choosen to obtain at least a computed point at each change of direction. The influence of the discretization and the distribution of the points is not treated in this article. For both strategies, the number of points is the same, but the length of the paths of the raster-pass and the swiping strategies is not the same. Therefore, the distribution of the points is different.

Raw measured data were the locations (*x*, *y*, *z*) of the nozzle as a function of time, allowing the calculation of speed, acceleration/deceleration and trajectory error in post-processing. The acquisition frequency of the (*x*, *y*, *z*) coordinates was about 83 Hz (time resolution of about 12 ms). A finite-difference scheme was used to calculate the speed, leading to a temporal resolution of about 24 ms. Note that throughout the manuscript, unless otherwise stated, we

mean by “speed” the *magnitude* of the speed vector. Finally, some parameters were fixed in the robot program for the whole study [34]. In particular, the *distance parameter CDIS*, defined by the robot manufacturer as the diameter around the programmed points of the trajectory through which the real trajectory must pass, was set to 5 mm. This value allows the robot to calculate the best trajectory between two side passes. The large number of passing points along the path allows to control the form deviation of the path.

the *velocity parameter CVEL*, playing a role in the control of the speed and acceleration of the robot, was set to 100%. Changing these values would obviously modify the quantitative results described in the following of the paper, but this does not change the conclusions of the study. Figure 4 shows the exact definition of the parameters.

KUKA System Variables

Syntax

`$APO={CVEL` *Velocity*`, CPTP` *DisPTP*`, CDIS` *DisCP*`, CORI` *Orientation*`}`

Explanation of the syntax

Element	Description
CVEL	Type: INT; unit: % Velocity parameter ■ **1 … 100** The approximation parameter specifies the percentage of the programmed velocity at which the approximate positioning process is started, at the earliest, in the deceleration phase towards the end point.
CPTP	Type: INT; unit: % Approximation distance for PTP and PTP spline motions (= furthest distance before the end point at which approximate positioning can begin) ■ **1 … 100** Explanation of the approximation parameter: (>>> "CPTP" Page 22) **Note**: PTP spline motions (SPTP) can be programmed in KUKA System Software 8.3 or higher.
CDIS	Type: REAL; unit: mm distance parameter Approximation starts, at the earliest, when the distance to the end point falls below the value specified here.
CORI	Type: REAL; unit: ° Orientation parameter Approximation starts, at the earliest, when the dominant orientation angle (rotation or swiveling of the longitudinal axis of the tool) falls below the angle distance to the end point specified here.

Fig. 4 Definition of parameters according [34]

Before presenting the results for the eight strategies, the next section is dedicated to preliminary observations on more elementary trajectories.

3. Preliminary observations

3.1 Impact of arc ON/OFF switching during a linear trajectory at constant nominal speed

This section is dedicated to the case of a simple straight trajectory at constant nominal speed. Figures 5-a-1 and -b-1 present a schematic view of the two experiments performed for a trajectory of 100 mm (from x = 0 mm to x = 100 mm). In the first case, the *arc ON* command is continuously activated. In the second case, a switch between *arc ON* and *arc OFF* is made at the mid-point of the trajectory. Although the nominal speed is constant, there are acceleration and deceleration phases in the actual movement of the nozzle. Figures 5-a-2 and -b-2 show the measured trajectories for a programmed nominal speed of 40 mm/s. Note that the scales of the x- and y- axes are different for readability. Whatever the *arc ON/OFF* choice, a transverse error in position ("backlash") is visible at the beginning and at the end of the toolpath: $y \approx 0.2$ mm and $y \approx -0.1$ mm respectively. A similar order of magnitude for the error is observed at the transition between *arc ON* and *arc OFF* in Fig. 5-b-2. In all cases, this transverse error (along y) is associated with an acceleration/deceleration of the nozzle: see Figs 5-a-3 and -b-3 showing the variation in time of the longitudinal speed. Errors also occur at the mid-point of the trajectory when switching from *arc ON* to *arc OFF*. The nozzle stops (zero speed) when switching from *arc ON* to *arc OFF*. Note that reverse switching (from *arc OFF* to *arc ON*) also leads to similar errors; see later in this paper. The total travel time is therefore longer when changing the status of the *arc ON/OFF* command due to the associated stops. Consequently, an inhomogeneous deposition of material is expected, due to the variation in speed while the WFS is constant. Note finally that, except in the transient sections of the trajectory (beginning, end and middle when switching from *arc ON* to *arc OFF*), the position error is limited to ±0.03 mm, which is very low.

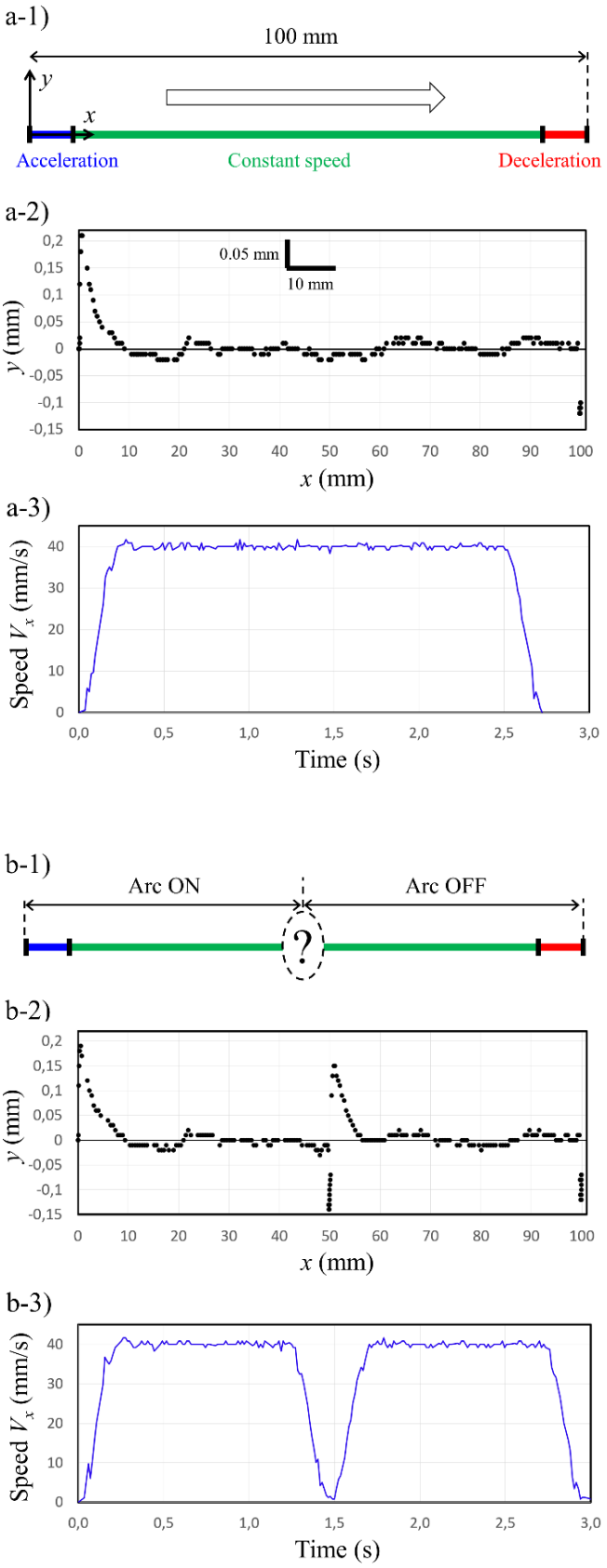

Fig. 5 Illustration of the influence of the *arc ON/OFF* command on the toolpath for a linear trajectory at a nominal speed of 40 mm/s: a) without changing the command, b) changing *arc ON* to *arc OFF* in the middle of the trajectory

3.2 Impact of a change in direction

This section deals with the influence of a sharp change in nozzle movement while the programmed nominal speed of the nozzle is constant. A sharp change induces a G1 discontinuity and does not present the progressiveness of a semi-circular toolpath. Figure 6-a illustrates the eight angles considered, namely between 2.95° (angle used in the swiping strategy) to 157.5° (angle used in the 45° triangular strategy). Deceleration and acceleration phases are obviously expected when changing direction; for instance, Figure 6-b shows the measured toolpath for a 45° angle and a nominal speed of 40 mm/s with *arc ON* activated over the whole trajectory. The toolpath appears to be curved close to the "vertex", with a maximum trajectory error of 1.62 mm. Figure 6-c provides the values of this error measured for the two nominal speeds (10 mm/s and 40 mm/s) and for the eight angles. Logically, the lower the nominal speed, the lower the trajectory error. It can be also seen that the lower the angle, the higher the error. For an angle of 2.95°, the error reaches 0.8 mm and 1.8 mm for 10 mm/s and 40 mm/s respectively, which is non-negligible. Finally, Figure 4-d gives first the average speeds measured over the whole trajectory (here about 2×43 mm in length) for the eight angles and the two nominal speeds. Values appear to be nearly constant because the durations of the curved sections are short in comparison with the total duration. They actually slightly decrease when the angle decreases (see in particular for 40 mm/s). Figure 6-d secondly gives the average speeds over the curved sections only. The curved section represents the transition between two line segments when the robot changes the pass, along the toolpath. To trim the curved section of the trajectory, two criteria are used. The first one considers that the curved section starts at the first measured point that is not aligned with the previous ones and ends at the last point that is not aligned with the following ones. A second criterion considers that the curved section is the section, for which the velocity is not constant. Thus, the impact of the angle is here significant, with speed values approximately halved between an angle of 157.5° and an angle of 2.95°. This may have significant consequences for strategies featuring numerous changes in direction, as will be discussed in Section 4.1 for the swiping strategy.

After these preliminary observations on simple cases, the next sections present the results for the different strategies presented in Section 2.2.

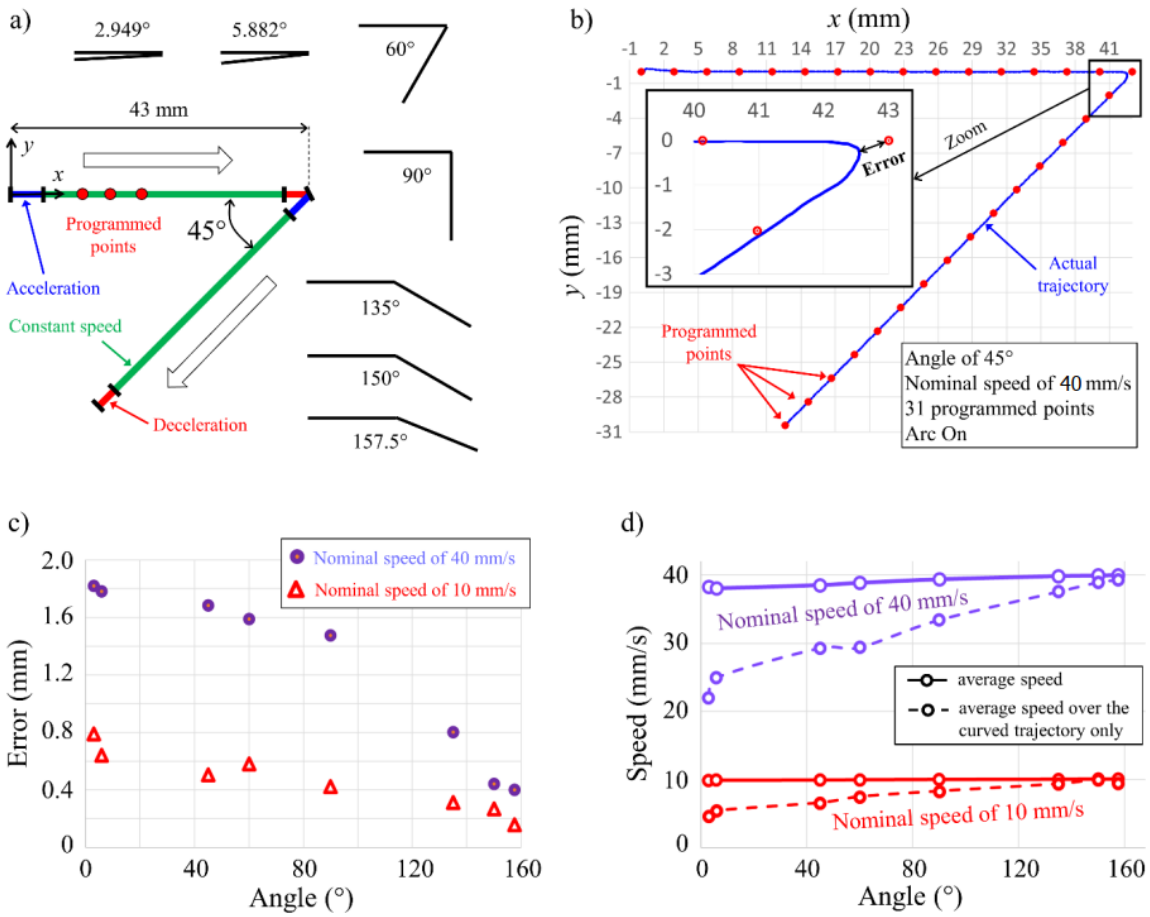

Fig. 6 Influence of the angle on a toolpath direction change: a) different angles considered and schematic representation for 45°, b) example of actual toolpath and definition of the error, c) error *vs.* angle for two nominal speeds of the robot, d) actual speeds achieved by the robot

4. Experimental results for the eight strategies

Tables A1 and A2 in the Appendix give an overview of the results for the eight strategies in Fig. 3 and the two nominal speeds (10 mm/s and 40 mm/s), for the small (21.5×43 mm^2) and large (43×86 mm^2) OR, respectively. The total time, the total length and the total volume of deposited material (*i.e.* when *arc ON* is activated) are presented. Two experimental protocols are applied: with *arc ON* activated over the whole toolpath; with *arc ON* and *OFF* inside and outside the OR respectively. The raster-pass strategy is a special case because *arc ON* and *arc OFF* are both applied inside the OR, leading to "non-applicable" (N/A) indicated in certain cells of the table. Furthermore, for the rectangular, spiral and swiping strategies, cells in the column "With *arc ON* and *OFF*" are indicated N/A because the whole toolpath remains in the OR. Various comments can be made when comparing the strategies. As it is not possible to

present all the toolpaths and speed graphs, some comparisons have been selected in the following three sections:

- Section 4.1 compares different strategies at the nominal speed of 40 mm/s for the small OR with *arc ON* activated over the whole trajectory. Only one of the triangular strategies (namely 60°) is presented in the illustrations for comparison, but other angles are also discussed.
- Section 4.2 discusses the difference depending on whether or not *arc OFF* is applied outside the OR.
- Section 4.3 compares the results between the two nominal speeds and between the small and large OR. This is illustrated by the 45° triangular strategy with *arc ON* activated over the whole trajectory.

4.1 Comparison between the different strategies at a nominal speed of 40 mm/s for the small OR

Firstly, Figure 7 presents the toolpaths and the speeds for the semi-circular, 60° triangular, rectangular and spiral strategies with *arc ON* activated over the whole trajectory, for a nominal speed of 40 mm/s and an OR of 21.5×43 mm^2. The red dots are the programmed points, whereas the blue curves correspond to the measured trajectories. The following comments can be made from this figure:

- As expected, all the changes in direction are accompanied by trajectory errors. This problem is significant for the quality of the WAAM process when the whole trajectory remains inside the OR (here for the rectangular and spiral strategies), because a local lack of material derives from the trajectory error. The problem is *a priori* not crucial when trajectory errors occur outside the OR (here for the semi-circular and 60° triangular strategies), but it can be observed that small curved sections of the toolpath also exist inside the OR, at its boundaries (when entering and leaving the OR). The comparison between the three triangular strategies (not reported here) shows that this problem increases with the angle from 45° to 90°. See later for considerations in terms of travel time.
- The time variations in nozzle speed are presented on the right side of Fig. 7. As expected, the speed decreases at each change in direction. The speed drop is of about 30% and 50% for the semi-circular and 60° triangular strategies respectively. The

comparison between the three triangular strategies (not reported here) shows that the lower the angle, the greater the speed drop. These drops are not *a priori* a problem as they occur mainly outside the OR (see below for considerations about the travel time). For the rectangular and spiral strategies for which the toolpath remains inside the OR, the speed drop is of about 25% at the direction changes, which is a problem for the homogeneity of the metal deposition. For all the small straight sections of the rectangular strategy as well as for the short section A-B of the spiral strategy, the robot has insufficient time to reach to the nominal speed (40 mm/s). Decreasing the nominal speed reduces these problems, as will be seen in Section 4.3.

- Table 1 allows a comparison of the four strategies presented in Fig. 7 in terms of total time, total length and average speed. By construction, the total time is shorter for the spiral and rectangular strategies than for the semi-circular and triangular strategies (because the latter have additional path sections, outside the OR), making the former advantageous from this point of view. The lowest total time is for the spiral strategy (5.628 s), which can be explained by the shortest total length. Note that 3 decimal places for the time measurements are considered, since the time stamp is 0.012 s (see Section 2.2). The rectangular strategy features a slightly longer total time (5.664 s) due to the slightly longer overall length. The accuracy of the toolpath can be defined by the ratio of the total length over the programmed length. The best accuracy is obtained for the semi-circular strategy (97%), due to the absence of sharp changes in direction (the programmed toolpath has smooth and curved transitions between the horizontal straight sections). However, the accuracies of all four strategies can be considered as being quite similar (between 95% and 97%).

Table 1. Comparison between the semi-circular, 60° triangular, rectangular and spiral strategies for a nominal speed of 40 mm/s and small OR (21.5×43 mm^2). For the triangular strategy, *arc ON* was activated over the whole toolpath

	Semi-circular	60° triangular	Rectangular	Spiral
Total time	6.264 s	6.456 s	5.664 s	5.628 s
Total length	234.201 mm	240.050 mm	207.618 mm	206.320 mm
Average speed	38.573 mm/s	38.349 mm/s	37.800 mm/s	37.902 mm/s
Total “programmed” length	242.603 mm	250.437 mm	217.600 mm	215.710 mm
Ratio between actual and programmed lengths	0.97	0.96	0.95	0.96

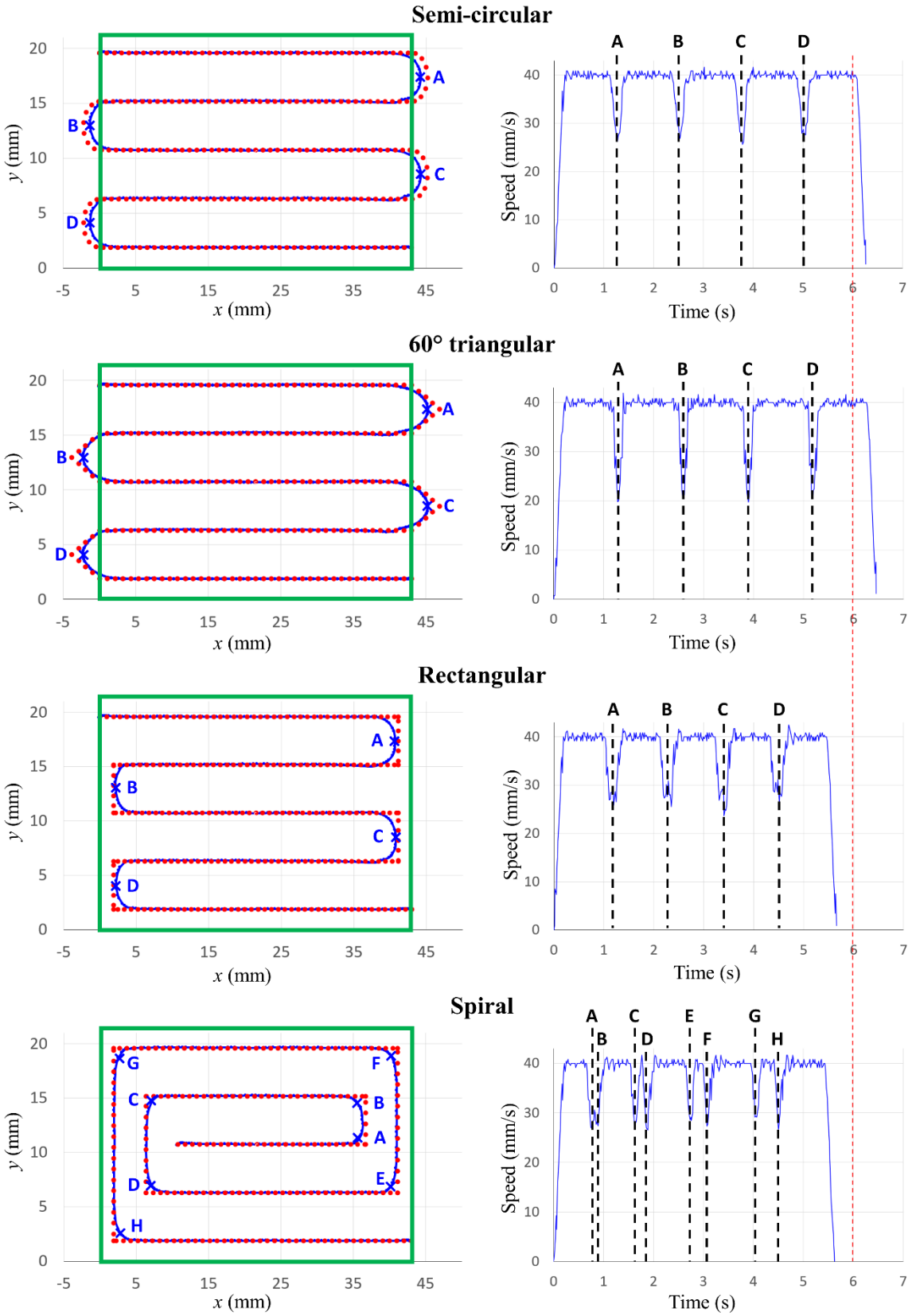

Fig. 7 Toolpath and speed for the semi-circular, rectangular and spiral strategies, as well as for one of the triangular strategies (namely 60°). The nominal speed was set to 40 mm/s and *arc ON* was activated over the whole of each trajectory

Secondly, Figure 8 compares the raster-pass and swiping strategies, still for a nominal speed of 40 mm/s and an OR of 21.5×43 mm^2. In addition to the trajectories and speeds, the figure also provides the variation in volume of deposited material (assuming a constant wire feed rate of 94.25 mm^3/s as indicated above) as a function of time and distance travelled. The following remarks can be made with respect to this figure:

- The sharp changes in direction lead to significant speed drops (see Figs 8-a-2 and -b-2): a drop of 100% and about 80% for the raster-pass and swiping strategies respectively. For the swiping strategy, this is accompanied by large trajectory errors of about 1.8 mm at the direction changes: see Fig. 8-b-1.
- Figures 8-a-3 and -b-3 show the variation in time of the volume of deposited material. Plateaus are obviously present when *arc OFF* is activated; to study the distribution of material on the part, it is necessary to construct figures a-4) and b-4) from figures a-3) and b-3), in order to obtain the volume of material deposited according to the curvilinear abscissa of the path and not according to time ; thus, negative consequences of the speed drops are visible: see zooms in Figs 8-a-4 and -b-4. The order of magnitude of the volume "jumps" is the same for the two strategies (about 7 mm^3).
- Table 2 enables a global comparison of the two strategies. The programmed and actual lengths as well as the volume of deposited material are higher for the swiping strategy than for the raster-pass strategy. This is due to the numerous weld bead overlap zones in the former case. The raster-pass strategy presents an accuracy (defined above as the ratio between total actual length and total programmed length) of 0.998. This good ratio is due to the fact that this strategy involves switches between *arc ON* and *arc OFF* at the beginning and end of each straight section: thus, the nozzle accurately reaches the end of each straight section (albeit while stopping). On the contrary, for the sweeping strategy, accuracy can be considered as low (length ratio of 0.89). This is due to an accumulation of trajectory error at each change in direction. Although over a much longer programmed length (464.246 mm compared to 387.910 mm), the total time for the swiping strategy is only slightly longer than that of the raster-pass strategy (12.036 s compared with 11.580 s). This is due to the time "lost" when switching between *arc ON* and *arc OFF* in the latter case.

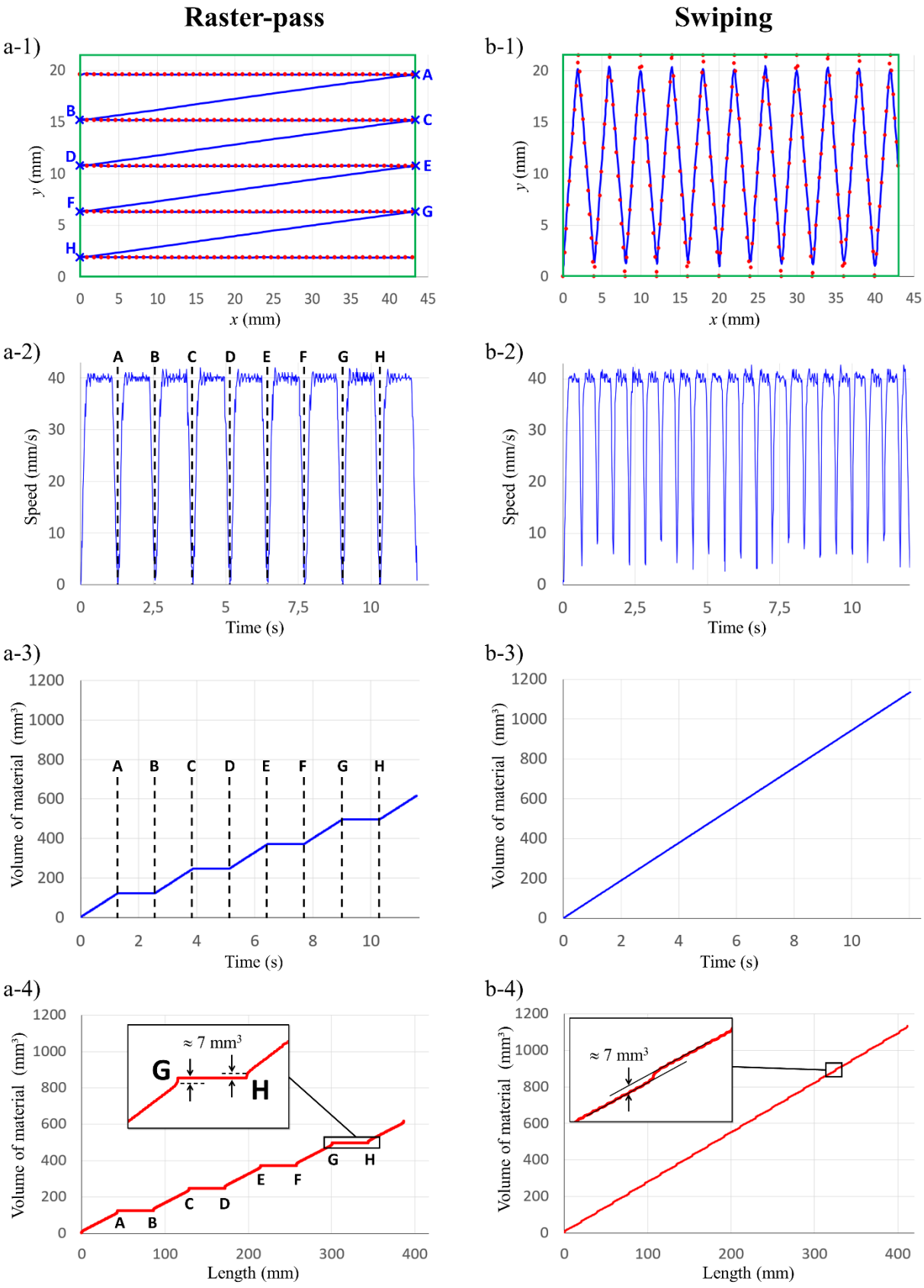

Fig. 8 Trajectory, speed and volume of materials for the raster-pass and swiping strategies, with a nominal speed of 40 mm/s

Table 2. Comparison between raster-pass and swiping strategies for a nominal speed of 40 mm/s and small OR (21.5×43 mm^2)

	Raster-pass	Swiping
Total time	11.580 s	12.036 s
Total length	386.971 mm	411.509 mm
Average speed	33.752 mm/s	34.725 mm/s
Volume of material deposited	615.133 mm^3	1134.389 mm^3
Total "programmed" length	387.910 mm	464.246 mm
Ratio between actual and programmed lengths	0.998	0.89

4.2 Difference depending on whether or not arc OFF is applied outside the OR

The objective of this section is to discuss the relevance of applying *arc OFF* outside the OR. First, Figure 9 illustrates the differences using a specific case for illustration purposes: the 45° triangular strategy at a nominal speed of 40 mm/s for an OR of 21.5×43 mm^2. Figures 9-a-1 and -b-1 show the toolpath in the two cases. The red and black dots correspond to the programmed points with *arc ON* and *arc OFF* respectively. The blue curves are the measured toolpaths as in the previous figures. Some comments can be made:

- the trajectory error is much higher outside the OR when *arc OFF* is activated (Fig. 9-a-1). When switching from *arc ON* to *arc OFF*, the speed drops to zero at times A, C, E and G (Fig. 9-a-2). Just after A, C, E and G, the speed is increased without reaching the nominal speed of 40 mm/s due to the transition from *arc OFF* to *arc ON* at times B, D, F and H. The nozzle stops were already observed in Section 3.1. The robot seems to correct the delay by cutting the programmed toolpath according to the programmed tolerance. One explanation may be that stopping the nozzle causes the robot axes to physically stop, while the controller continues to follow the programmed path. In this case, the actual path is caught up when the robot axes are released. The resulting speed law is thus a combination of the kinematic behavior of the robot and the interaction between CMT equipment and robot controllers. The delays (acceleration and deceleration times) due to *arc ON/OFF* switching appear to be compensated for by a shorter toolpath outside the OR.
- The speed reductions when *arc ON* is activated over the whole trajectory (Fig. 9-b-2) are of higher amplitudes than those observed for the 60° triangular strategy in Fig. 7: the smaller the angle, the greater the speed drop.

- As in Section 4.1, variations in the volume of deposited material assuming a constant WFS are displayed in Figs 9-a-3 and -b-3 as a function of time, and in Figs 9-a-4 and -b-4 as a function of the distance travelled. The order of magnitude of the volume "jumps" are the same for the two strategies (about 7 mm^3), but it is less problematic when *arc ON* is activated over the whole trajectory because it occurs outside the OR (see Figs. 9-b-1 and -b-4).

Table 3 provides a quantitative comparison showing various output parameters. Times and lengths were measured over different phases of the trajectory: constant speed in the OR, acceleration in the OR; deceleration in the OR; inside the OR; outside the OR; and over the whole toolpath. It can be noted that a "total time with *arc OFF* inside the OR" is indicated, which may appear strange because, in theory, *arc OFF* is activated only when reaching the boundary of the OR. Indeed, (small) time shifts are observed in the application of the *arc ON/OFF* command. The following comments can be made from the table:

- When *arc ON* is activated over the whole trajectory, the time of the whole toolpath is shorter (6.732 s to be compared with 7.932 s), which is advantageous for productivity. Moreover, the total time *at constant speed* inside the OR is longer (4.632 s compared to 4.380 s), which is *a priori* better in terms of deposition quality inside the OR.
- The same remarks can be made about the lengths, but differences can be highlighted about the times *outside* the OR. To make up for the delay due to the activation of the *arc OFF* command, the toolpath length is in practice much shorter (see Fig. 9-a-1). This leads to shorter lengths outside the OR (19.474 mm, compared to 34.920 mm).
- The total time with "*arc OFF* inside the OR" is 0.156 s, which corresponds to about 2% of the duration of the whole toolpath (7.932 s). This cannot be considered as a negligible parasitic effect in the case of large mechanical parts.

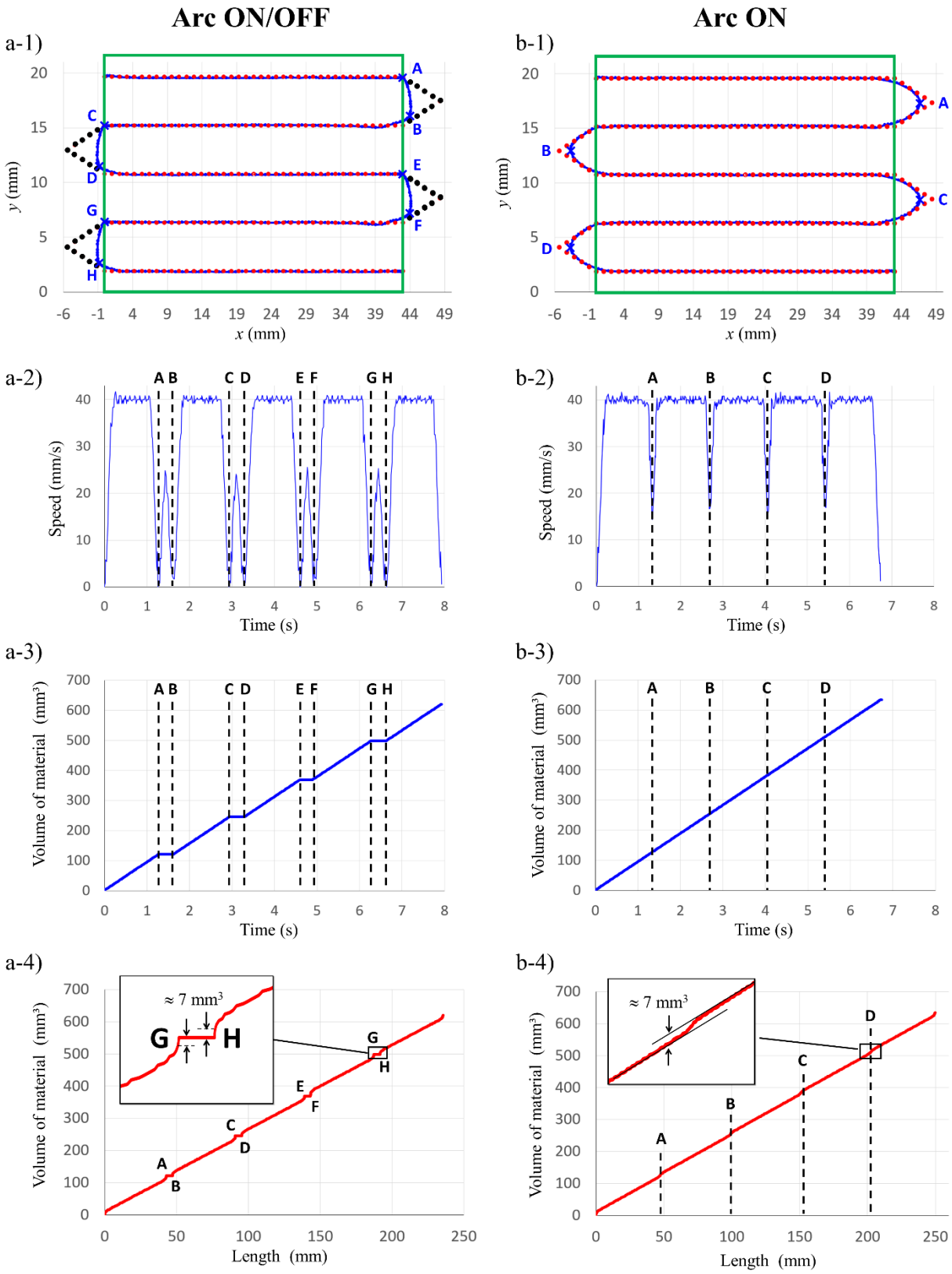

Fig. 9 Influence of the *arc ON/OFF* command on the trajectory for the 45° triangular and a nominal speed of 40 mm/s: a) with *arc ON* and *OFF* inside and outside the objective rectangle respectively, b) with *arc ON* activated over the whole toolpath

Table 3. Influence of the *arc ON/OFF* command for the 45° triangular strategy, with a nominal speed of 40 mm/s and small OR (21.5×43 mm^2)

		With *arc OFF* outside the OR	With *arc ON* over the whole toolpath
Total time	at constant speed in the OR	4.380 s	4.632 s
	of acceleration in the OR	0.780 s	0.468 s
	of deceleration in the OR	0.972 s	0.480 s
	with *arc OFF* inside the OR	0.156 s	N/A
	inside the OR	6.288 s	5.580 s
	outside the OR	1.644 s	1.152 s
	of the whole toolpath	**7.932 s**	**6.732 s**
Total length	at constant speed in the OR	175.442 mm	185.470 mm
	of acceleration in the OR	22.528 mm	14.492 mm
	of deceleration in the OR	17.900 mm	14.975 mm
	with *arc OFF* inside the OR	0.205 mm	N/A
	inside the OR	216.075 mm	214.937 mm
	outside the OR	19.474 mm	34.920 mm
	of the whole toolpath	**235.549 mm**	**249.857 mm**
Total "programmed" length		261.301 mm	261.301 mm
Total volume of material deposited		**619.788 mm^3**	**634.489 mm^3**

4.3 Comparison between the two nominal speeds and the two OR areas

Table 4 compares the results between the two nominal speeds (10 mm/s and 40 mm/s) and between the two OR areas (21.5×43 mm^2 and 43×86 mm^2). The comparison concerns the 45° triangular strategy with *arc ON* activated over the whole trajectory. Some comments can be advanced about the ratios of results between the two nominal speeds and between the two areas:

- At a nominal speed of 10 mm/s, the ratio of total times is equal to 3.68 between the two sizes of OR. It is equal to 3.70 for the total length. Thus, the robot took 3.68 times longer to cover a 3.70 times longer toolpath, which shows a nearly linear response. However, at a nominal speed of 40 mm/s, the robot took 3.61 times longer to cover a 3.76 times longer toolpath, highlighting a loss of proportionality.
- Concerning this difference ratio of 0.25 between the two nominal speeds, it can be noted that proportionality is clearly respected: the measured time ratio is of 0.26 and 0.25 for small and large OR respectively. When multiplying the nominal speed by

four, the travel length is lower: a decrease of 3% and 2% for the small and large OR respectively, which is not negligible.

Table 4. Comparison between two OR areas and two nominal speeds for the 45° triangular strategy with *arc ON* activated over the whole toolpath

		OR of **21.5×43 mm^2**	OR of **43×86 mm^2**	Time ratio between the two sizes	Length ratio between the two sizes
10 mm/s	Time	26.280 s	96.624 s	3.68	
	Length	258.896 mm	958.865 mm		3.70
40 mm/s	Time	6.732 s	24.300 s	3.61	
	Length	249.857 mm	938.206 mm		3.76
Time ratio between the two speeds		0.26	0.25		
Length ratio between the two speeds		0.97	0.98		

Before proposing a manufacturing time model in Section 5, Table A3 in the Appendix provides the results for all the strategies considered in this study, for completeness.

4.4 Additional experiments

Finally, experiments were duplicated at 15 various locations in the work space (see schematic view in Fig. 10). Indeed, a serial robot features *a priori* variable structural stiffness within its workspace [35], and the magnitudes of trajectory errors may vary inside that workspace. The results described in the previous sections corresponded to location "A". Let us mention that the robot is not placed symmetrically with respect to the work space, justifying the choice of testing symmetrical locations in the chamber. At each location, a trajectory was performed using the swiping strategy and a nominal speed of 20 mm/min. As in the previous sections, two OR areas were considered: 21.5×43 mm^2 and 43×86 mm^2. For the small OR, the deposition time varied between 23.840 s and 23.890 s depending on the location in the work space. For the large one, it varied between 92.964 s and 92.988 s. In conclusion, deposition times can be considered as homogeneous within the work space. The same conclusion can be made from the values of the lengths: there is no significant variation between the locations. These results are positive, as they do not reveal any heterogeneity in the workspace of the robot.

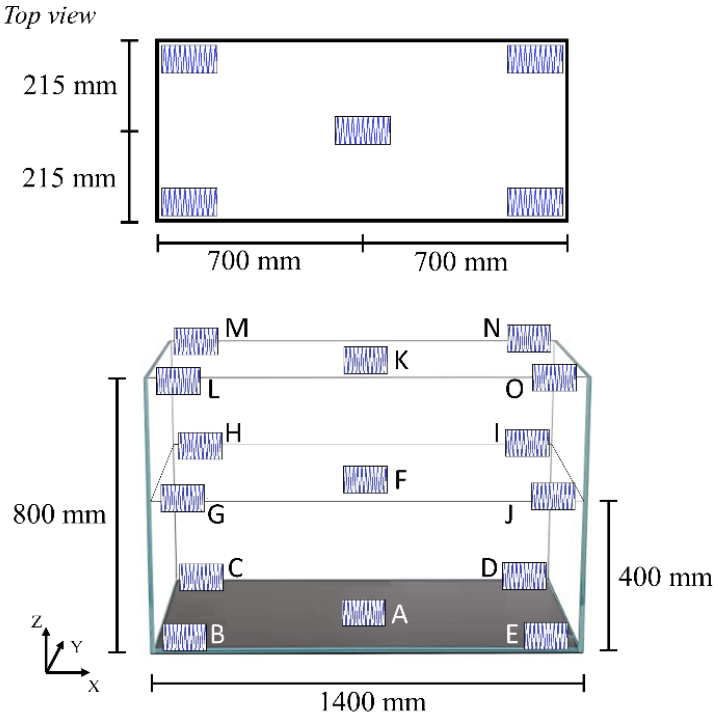

Fig. 10 Schematic view of the inert chamber with the locations of the different zones in which the same swiping depositions were performed

4.5 General comments

After presenting and analyzing the results of the experimental tests, some general comments highlight the fact that compromises have to be found between various aspects. From the preliminary study in Section 3.1 (linear trajectory at constant nominal speed), *arc ON/OFF* switching has two drawbacks which may induce material defects: a "backlash" (due to clearance within the joints of the robots) and a robot stop (accompanied by deceleration/acceleration phases). For these reasons, in the context of the WAAM process, the use of discontinuous deposition should be *a priori* avoided for quality purposes. From the preliminary study in Section 3.2 (impact of a sharp change in direction), it appears that the robot fails to maintain a constant speed as expected in *CVEL* mode, leading to an error in both speed and position. The sharper the angle, the slower the robot movement in the transition zones, and the higher the trajectory error. As a general remark, sharp angles should be avoided. In Section 4.2, the toolpath with *arc ON* over the whole trajectory was more accurate (see Table 4). This may appear contradictory with the previous comments because no robot stops occur when leaving/entering the OR. In fact, the delays (caused by the stops when

leaving/entering the OR) when using *arc OFF* outside the OR appeared to be corrected by the controller by cutting the trajectory in the curves (see Fig. 9-a-1), leading to a large trajectory error. However, this is not *a priori* a problem because this cutting occurs outside the OR.

Various remarks can be made about the comparison between the eight strategies in Section 4.1:

- The advantage of the raster-pass strategy is the high accuracy of the toolpath, because all the deposition sections are along straight lines with robot stops at each ends (due to the switching between *arc ON* and *arc OFF*). However, from the production point of view, the raster-pass strategy is not efficient. A large part of the time is non-productive, consuming resources (energy, time, others).
- The semi-circular strategy presents the lowest error between programmed total length and measured total length. This toolpath is also the one with the highest average speed. These two characteristics have a direct positive impact on the quality of the deposition.
- The swiping strategy has the lowest ratio between actual and programmed lengths. This means that the robot does not perform the programmed toolpath completely.

Discontinuous deposition would be relevant when adding extra lengths outside the "nominal" OR, leading in practice to a larger deposition zone. These extra lengths should correspond to acceleration and deceleration phases measured on straight trajectory sections. For instance, for a nominal speed of 40 mm/s and the 45° triangular strategy with *arc OFF* outside the OR, these distances can be estimated at 4.5 mm for the acceleration phases (just before entering the nominal OR) and 3.6 mm for the deceleration phases (just after leaving the nominal OR). By construction, these values are smaller when *arc ON* is activated over the whole trajectory.

The data collected from the swiping experiments at different locations revealed that there is repeatability with respect to the deposition times and total deposition lengths (see Section 4.4). It is therefore possible to apply formulas to calculate the deposition time independently of the location within the work space.

5. Time estimation model

Based on the results of the experiments, a manufacturing time estimation model is now proposed to calculate the manufacturing time of any $W \times L$ area of OR from a limited number of previously-identified parameters for a single area. The method is illustrated for the 45° triangular strategy, but the principle is the same for the other strategies. Based on the results of the experiments at 10 mm/s and 40 mm/s, Table 5 provides the parameters initially identified for the small OR (21.5×43 mm^2), distinguishing whether *OFF arc* is applied outside the OR or not.

- $T_{\text{init accel}}$ and $L_{\text{init accel}}$ are the time and the length, respectively, of the initial acceleration;
- L_{accel} and L_{decel} are the lengths of acceleration and deceleration (respectively) at the beginning and end (respectively) of a horizontal straight section of the toolpath excluding the first and last ones. It can be noted in Table 5 that some values are equal to zero, meaning that acceleration or deceleration phases do not occur in the horizontal straight sections (they are in transitions in between);
- T_{trans}: time of the transition between two successive horizontal sections of toolpath;
- $T_{\text{final decel}}$ and $L_{\text{final decel}}$ are the time and the length, respectively, of the final deceleration.

Table 5. Parameters identified for the 45° triangular strategy with the small OR (21.5×43 mm^2), to be used in Equations (3-7) for time calculation

	Nominal speed (TS)			
	10 mm/s		40 mm/s	
	With *arc ON* over the whole toolpath	With *arc OFF* outside the OR	With *arc ON* over the whole toolpath	With *arc OFF* outside the OR
$T_{\text{init accel}}$	0.144 s	0.144 s	0.204 s	0.216 s
$L_{\text{init accel}}$	0.617 mm	0.610 mm	4.212 mm	4.944 mm
L_{decel}	0 mm	0.876 mm	2.500 mm	3.670 mm
L_{accel}	0 mm	0 mm	2.200 mm	4.387 mm
T_{trans}	1.200 s	1.410 s	0.426 s	0.408 s
$L_{\text{final decel}}$	0.806 mm	0.807 mm	3.862 mm	3.807 mm
$T_{\text{final decel}}$	0.180 s	0.180 s	0.192 s	0.192 s

Let us note that parameters $T_{\text{init accel}}$, $L_{\text{init accel}}$, $T_{\text{final decel}}$ and $L_{\text{final decel}}$ were measured from the median of several experiments with different strategies (they are not specific to the 45° triangular strategy). On the contrary, as L_{accel}, L_{decel} and T_{trans} are specific to the strategy considered, we measured them for the 45° triangular strategy (one experiment).

The following formula can then be used to calculate the total time as a function of the $W \times L$ area of the OR, the nominal speed (TS) and the number of horizontal weld beads n_{WB} calculated from Eqs (1) and (2):

$$T_{\text{total}}(W, L, TS, n_{\text{WB}}) = T_{\text{init accel}}(TS) + T_{\text{init const}}(L, TS) + (n_{\text{WB}} - 1) \times T_{\text{trans}}(TS) + (n_{\text{WB}} - 2) \times T_{\text{straight const}}(L, TS) + T_{\text{final const}}(L, TS) + T_{\text{final decel}}(TS) \quad (3)$$

where:

- $T_{\text{init const}}$ is the duration of the first horizontal straight section at constant speed:

$$T_{\text{init const}} = \frac{L - L_{\text{init accel}}(TS) - L_{\text{decel}}(TS)}{TS} \quad (4)$$

- $T_{\text{straight const}}$ is the duration of any horizontal straight section at constant speed, excluding the first and final ones:

$$T_{\text{straight const}} = \frac{L - L_{\text{accel}}(TS) - L_{\text{decel}}(TS)}{TS} \quad (5)$$

- $T_{\text{final\_const}}$ is the duration of the final horizontal straight section at constant speed:

$$T_{\text{final const}} = \frac{L - L_{\text{accel}}(TS) - L_{\text{final decel}}(TS)}{TS} \quad (6)$$

As an evaluation of the accuracy of the formula, numerical applications were performed to calculate the total times for the large OR (W = 43 mm and L = 86 mm) from the parameters identified for the small OR. They give:

- <u>for TS = 10 mm/s and *arc ON* over the whole trajectory:</u> 96.982 s, *i.e.* 0.38% of error with respect with measured value (96.612 s, see Table A2 in Appendix);
- <u>for TS = 10 mm/s and *arc OFF* outside the OR:</u> 98.081 s, *i.e.* 2.28% of error with respect with measured value (100.368 s);
- <u>for TS = 40 mm/s and *arc ON* over the whole trajectory:</u> 24.304 s, *i.e.* 0.03% of error with respect with measured value (24.312 s);

- for TS = 40 mm/s and *arc OFF* outside the OR: 23.544 s, *i.e.* 16.3% of error with respect with measured value (28.128 s).

The same approach was adopted to calculate the total times for the small OR from the parameters identified for the large OR. This gives 0.24%, 3.5%, 0.33% and 9.3% of error respectively (calculation not reported here). Thus we consider that the formula is precise for all the cases with *arc ON* activated over the whole trajectory: the errors are less than 0.4%. The error is higher with *arc OFF* activated outside the OR: up to 16.3%. This is mainly due to the assessment of L_{accel}, L_{decel} and T_{trans} which was performed from one experiment, as noted above. This highlights the importance of the preliminary assessment of these parameters when using the manufacturing time model.
This model can be used to simulate the deposit of simple rectangular shapes. But a complex shape can also be treated, if it is possible to split it into a set of rectangular shapes. Moreover, the model is based on the separation of the path into straight segments and connections. Any path formed by these two elementary shapes can be evaluated. Further work is expected to evaluate the model against more complex curved paths.

6. Conclusion

In the WAAM process, the accuracy of the toolpath is of prime importance for the mechanical properties of the final part because of the material defects that could be generated. This accuracy depends on the kinematic behavior of the robot, as well as the interaction between CMT equipment and robot controllers. Beyond the cases treated in this paper and the chosen test conditions (speeds, dimensions...), this type of study shows that a kinematic analysis of the robot's behavior brings valuable information for off-line trajectory programming. It is possible to build rules that can be used by the manufacturer to correctly program the trajectory before building a part.

A motion analysis of the nozzle using a KUKA KR 100-2 HA 2000 robot with a KRC2 controller was performed in this study. The movement of the nozzle was analyzed without depositing material (trajectory definition only) using various strategies, nozzle speeds and layer areas for continuous and discontinuous "virtual" depositions. The analysis also enabled us to identify various problems associated with acceleration and deceleration phases, in particular for discontinuous depositions. Several points can be highlighted:

- Discontinuous deposition leads to additional travel time, due to deceleration and acceleration at each deposition stop and restart respectively. However, it has the advantage of saving material (in sections intended to be transient).
- Planning sections of the toolpath outside the nominal deposition area can be useful to "move" inaccuracy problems to where they are not critical from a material quality perspective. Discontinuous deposition would be relevant when adding extra lengths outside the nominal deposition area, leading in practice to a larger deposition zone. These extra lengths should correspond to acceleration and deceleration phases measured on straight trajectory sections. Deposition outside the nominal deposition area may also be relevant, but it requires additional conventional machining time and tooling.
- The swiping strategy is the most commonly-used but it has limits and is not applicable to all cases. It can be useful to have other strategies, as proposed in this paper. Sharp changes in direction in the programmed toolpath actually lead to a trajectory error. Thus the semi-circular strategy (G1 continuous) enables this accuracy problem to be lessened.
- It is possible to define manufacturing time estimation models taking into account acceleration and deceleration phases. However, stopping deposition outside the nominal deposition area requires precise parameter identification for a correct calculation of the manufacturing time.

As a general comment from the above points, compromises must therefore be found. Based on the tests performed in this study, the semi-circular strategy appears to be the most relevant in the case of continuous deposition over the whole toolpath. Perspectives of the study include the consideration of cooling in the definition of in-plane and inter-layer trajectories.

Declarations

Funding

This work was supported by the French Research Agency through the Indus Addi project (N° ANR-19-CE10-0001-01).

Competing Interests

The authors declare no competing of interest.

Data Availability

The datasets generated during and/or analyzed during the current study are available from the corresponding author on reasonable request.

Author contribution

R. Viola Da Silva: Conceptualization, Methodology, Validation, Formal analysis, Software, Investigation, Data curation, Writing - original draft, Writing - review & editing, Visualization.

X. Balandraud: Conceptualization, Methodology, Validation, Formal analysis, Writing - review & editing, Visualization, Supervision.

F. Poulhaon: Conceptualization, Methodology, Validation, Formal analysis, Resources, Writing - review & editing, Supervision.

P. Michaud: Conceptualization, Methodology, Formal analysis, Resources, Writing - review & editing, Project administration.

E. Duc: Conceptualization, Methodology, Formal analysis, Resources, Writing - review & editing, Project administration, Funding acquisition.

Compliance with ethical standards N/A

References

1. Dinovitzer M, Chen XH, Laliberte J, Huang X, Frei H, (2019) Effect of wire and arc additive manufacturing (WAAM) process parameters on bead geometry and microstructure. Addit Manuf 26:138–146. https://doi.org/10.1016/j.addma.2018.12.013
2. McAndrew AR, Rosales MA, Colegrove PA, Honnige JR, Ho A, Fayolle R, Eyitayo K, Stan I, Sukrongpang P, Crochemore A, Pinter Z (2018) Interpass rolling of Ti-6Al-4V wire + arc additively manufactured features for microstructural refinement. Addit Manuf 21:340–349. https://doi.org/10.1016/j.addma.2018.03.006
3. Williams SW, Martina F, Addison AC, Ding J, Pardal G, Colegrove P (2016) Wire plus Arc Additive Manufacturing. Mater Sci Technol 32:641–647. https://doi.org/10.1179/1743284715Y.0000000073
4. Ding DH, Pan ZX, Cuiuri D, Li HJ (2015) Process planning for robotic wire and arc additive manufacturing, In: IEEE (ed) Proceedings of the 2015 10th IEEE Conference on Industrial Electronics and Applications. IEEE Conference on Industrial Electronics and Applications. IEEE, New York, pp 1994–1997. https://doi.org/10.1109/ICIEA.2015.7334441
5. Fuchs C, Baier D, Semm T, Zaeh MF (2020) Determining the machining allowance for WAAM parts. Prod Eng Res Devel 14:629–637. https://doi.org/10.1007/s11740-020-00982-9

6. Almeida PMS, Williams S (2010) Innovative process model of Ti-6Al-4V additive layer manufacturing using cold metal transfer (CMT). In: 21st Annual International Solid Freeform Fabrication Symposium: An Additive Manufacturing Conference. 9–11 August 2010, Austin, Texas, USA. University of Texas. https://doi.org/10.26153/tsw/15162
7. Li JH, Zhou XL, Meng QB, Brochu M, Chekir N, Sixsmith JJ, Hascoet JY, Zhao ZF (2021) Deterministic modeling of solidification microstructure formation in directed energy deposition fabricated Ti6Al4V. Addit Manuf 46:102182. https://doi.org/10.1016/j.addma.2021.102182
8. Evjemo LD, Moe S, Gravdahl JT (2020) Robotised wire arc additive manufacturing using set-based control: experimental results. In: IFAC-PapersOnLine, vol. 53(2), pp. 10044-10051. 21st IFAC World Congress on Automatic Control - Meeting Societal Challenges, Elsevier, Amsterdam, Netherland. https://doi.org/10.1016/j.ifacol.2020.12.2725
9. Jafari D, Vaneker THJ, Gibson I (2021) Wire and arc additive manufacturing: opportunities and challenges to control the quality and accuracy of manufactured parts. Mater Des 202:109471. https://doi.org/10.1016/j.matdes.2021.109471
10. Ferreira RP, Scotti A (2021) The concept of a novel path planning strategy for wire plus arc additive manufacturing of bulky parts: pixel. Metals 11:498. https://doi.org/10.3390/met11030498
11. Michel F, Lockett H, Ding J, Martina F, Marinelli G, Williams S (2019) A modular path planning solution for Wire + Arc Additive Manufacturing. Robot Comput-Integr Manuf 60:1–11. https://doi.org/10.1016/j.rcim.2019.05.009
12. Thompson B, Yoon HS (2014) Efficient path planning algorithm for additive manufacturing systems. IEEE Trans Compon Packag Manuf Technol 4:1555–1563. https://doi.org/10.1109/TCPMT.2014.2338791
13. Zhao Y, Li F, Chen SJ, Lu ZY (2019) Unit block-based process planning strategy of WAAM for complex shell-shaped component, Int J Adv Manuf Technol 104:3915–3927. https://doi.org/10.1007/s00170-019-04141-y
14. Chokkalingham S, Chandrasekhar N, Vasudevan M (2012) Predicting the depth of penetration and weld bead width from the infra red thermal image of the weld pool using artificial neural network modeling. J Intell Manuf 23:1995–2001. https://doi.org/10.1007/s10845-011-0526-4

15. Cunningham CR, Flynn JM, Shokrani A, Dhokia V, Newman ST (2018) Invited review article: Strategies and processes for high quality wire arc additive manufacturing. Addit Manuf 22:672–686. https://doi.org/10.1016/j.addma.2018.06.020
16. Bertoldi M, Yardimci MA, Pistor CM, Guceri SI (1998) Domain decomposition and space filling curves in toolpath planning and generation. In: Marcus HL, Beaman JJ, Bourell DL, Barlow JW, Crawford RH (eds) Solid Freeform Fabrication Proceedings, August 1998, Solid Freeform Fabrication Proceedings (Series). Univ Texas Austin, Austin, RX, USA, pp 267–274. https://doi.org/10.26153/tsw/608
17. Yang Y, Loh HT, Fuh JYH, Wang YG (2002) Equidistant path generation for improving scanning efficiency in layered manufacturing. Rapid Prototyp J 8:30–37. https://doi.org/10.1108/13552540210413284
18. Zhang YM, Chen YW, Li PJ, Male AT (2003) Weld deposition-based rapid prototyping: a preliminary study. J Mater Process Technol 135:347–357. https://doi.org/10.1016/S0924-0136(02)00867-1
19. Ding DH, Pan ZX, Cuiuri D, Li HJ (2015) A practical path planning methodology for wire and arc additive manufacturing of thin-walled structures. Robot Comput-Integr Manuf 34:8–19. https://doi.org/10.1016/j.rcim.2015.01.003
20. Schmitz M, Wiartalla J, Gelfgren M, Mann S, Corves B, Husing M (2021) A Robot-Centered Path-Planning Algorithm for Multidirectional Additive Manufacturing for WAAM Processes and Pure Object Manipulation. Appl Phys Basel 11:5759. https://doi.org/10.3390/app11135759
21. Aldalur E, Veiga F, Suárez A, Bilbao J, Lamikiz A (2020) High deposition wire arc additive manufacturing of mild steel: Strategies and heat input effect on microstructure and mechanical properties. J Manuf Process 58:615–626. https://doi.org/10.1016/j.jmapro.2020.08.060
22. Liu XM, Qiu CR, Zeng QF, Li AP (2019) Kinematics analysis and trajectory planning of collaborative welding robot with multiple manipulators, In: P. Butala, E. Goverak, R. Vrabic (eds) 52nd CIRP Conference on Manufacturing Systems (CMS), Procedia CIRP, vol. 81. Elsevier, Amsterdam, Netherland, pp 1034–1039. https://doi.org/10.1016/j.procir.2019.03.247
23. Jin GQ, Li WD, Gao L (2013) An adaptive process planning approach of rapid prototyping and manufacturing. Robot Comput-Integr Manuf 29:23–38. https://doi.org/10.1016/j.rcim.2012.07.001

24. Rauch M, Nwankpa UV, Hascoet JY (2021) Investigation of deposition strategy on wire and arc additive manufacturing of aluminium components. J Adv Joining Process 4:100074. https://doi.org/10.1016/j.jajp.2021.100074

25. Srivastava M., Rathee S., Tiwari A., Dongre M. (2023) Wire arc additive manufacturing of metals: A review on processes, materials and their behavior. Materials Chemistry and Physics 294 126988

26. Lim W.S, Dharmawan A.G, Soh G.S (2022) Development and performance evaluation of a hybrid-wire arc additive manufacturing system based on robot manipulators. Materials Today: Proceedings 70 587–592

27. Ding DH, Pan ZX, Cuiuri D, Li HJ (2014) A tool-path generation strategy for wire and arc additive manufacturing. Int J Adv Manuf Technol 73:173–183. https://doi.org/10.1007/s00170-014-5808-5

28. Diourté A, Bugarin F, Bordreuil C, Segonds S (2021) Continuous three-dimensional path planning (CTPP) for complex thin parts with wire arc additive manufacturing. Addit Manuf 37:101622. https://doi.org/10.1016/j.addma.2020.101622

29. Li F, Chen SJ, Shi JB, Zhao Y, Tian HY (2018) Thermoelectric cooling-aided bead geometry regulation in wire and arc-based additive manufacturing of thin-walled structures. Appl Sci Basel 8:207. https://doi.org/10.3390/app8020207

30. Geng HB, Li JL, Xiong JT, Lin X (2017) Optimisation of interpass temperature and heat input for wire and arc additive manufacturing 5A06 aluminium alloy. Sci Technol Weld Joining 22:472–483. https://doi.org/10.1080/13621718.2016.1259031.

31. Zhao Y, Jia YZ, Chen SJ, Shi JB, Li F (2020) Process planning strategy for wire-arc additive manufacturing: thermal behavior considerations. Addit Manuf 32:100935. https://doi.org/10.1016/j.addma.2019.100935

32. KUKA.RobotSensorInterface 3.1 – For KUKA System Software 8.2, Issued: 23.12.2010, Version: KST RSI 3.1 V1 en. KUKA Roboter GmbH, Augsburg, Germany, 2010. http://supportwop.com/IntegrationRobot/content/6-Syst%C3%A8mes_int%C3%A9grations/RobotSensorInterface/KST_RSI_31_en.pdf. Accessed 28 October 2022

33. Nguyen L, Buhl J, Bambach M (2020) Continuous Eulerian toolpath strategies for wire-arc additive manufacturing of rib-web structures with machine-learning-based adaptive void filling. Addit Manuf 35:101265. https://doi.org/10.1016/j.addma.2020.101265

34. Expert Documentation. System Variables. For KUKA System Software 8.1, 8.2, 8.3 and 8.4. Version: KSS 8.1, 8.2, 8.3, 8.4 System Variables V2. Issued: 26.09.2016, KUKA Roboter GmbH, Augsburg, Germany, 2016.

35. Sun JB, Zhang WM, Liu ZH (2018) Translation Stiffness Calculation for Serial Robots. In: ICRAI 2018: Proceedings of 2018 4th International Conference on Robotics and Artificial Intelligence. Assoc Computing Machinary, New York, USA, pp 87-91. https://doi.org/10.1145/3297097.3297103

Table A1 (Appendix). Comparison between different strategies and two nominal speeds for the small OR (21.5×43 mm^2). Measured parameters are the total time and length over the whole toolpath, as well as the total volume of material deposited (i.e. when *arc ON* is activated).

Strategy	Nominal speed	Measured parameter	With *arc ON* over the whole toolpath	With *arc OFF* outside the OR	
				Over the whole toolpath	When *arc* is *ON*
Raster-pass	10 mm/s	Time	N/A	40.644 s	22.38 s
		Length	N/A	387.900 mm	215.084 mm
		Volume	N/A	2118.353 mm^3	2108.176 mm^3
	40 mm/s	Time	N/A	11.580 s	6.408 s
		Length	N/A	386.971 mm	214.712 mm
		Volume	N/A	615.133 mm^3	605.083 mm^3
Triangular 45°	10 mm/s	Time	26.280 s	27.972 s	22.152 s
		Length	258.896 mm	259.877 mm	215.642 mm
		Volume	2476.881 mm^3	2159.070 mm^3	2085.557 mm^3
	40 mm/s	Time	6.732 s	7.932 s	6.132 s
		Length	249.857 mm	235.549 mm	215.870 mm
		Volume	634.489 mm^3	619.788 mm^3	577.939 mm^3
Triangular 60°	10 mm/s	Time	25.212 s	26.856 s	22.152 s
		Length	248.426 mm	249.427 mm	215.889 mm
		Volume	2376.223 mm^3	2165.724 mm^3	2085.557 mm^3
	40 mm/s	Time	6.456 s	8.172 s	6.096 s
		Length	240.050 mm	242.118 mm	215.360 mm
		Volume	608.476 mm^3	615.264 mm^3	574.546 mm^3
Triangular 90°	10 mm/s	Time	24.156 s	25.848 s	22.068 s
		Length	238.759 mm	239.893 mm	215.354 mm
		Volume	2276.695 mm^3	2161.332 mm^3	2082.164 mm^3
	40 mm/s	Time	6.180 s	7.932 s	6.132 s
		Length	230.613 mm	235.549 mm	215.870 mm
		Volume	582.463 mm^3	613.002 mm^3	577.939 mm^3
Rectangular	10 mm/s	Time	21.936 s	N/A	N/A
		Length	215.997 mm	N/A	N/A
		Volume	2067.461 mm^3	N/A	N/A
	40 mm/s	Time	5.664 s	N/A	N/A
		Length	207.618 mm	N/A	N/A
		Volume	533.830 mm^3	N/A	N/A
Semi-circular	10 mm/s	Time	24.384 s	26.136 s	21.840 s
		Length	242.306 mm	243.187 mm	212.385 mm
		Volume	2298.184 mm^3	2110.440 mm^3	2057.282 mm^3
	40 mm/s	Time	6.264 s	7.908 s	6.108 s
		Length	234.201 mm	237.967 mm	212.722 mm
		Volume	590.380 mm^3	607.347 mm^3	576.808 mm^3
Spiral	10 mm/s	Time	21.720 s	N/A	N/A
		Length	214.383 mm	N/A	N/A
		Volume	2047.103 mm^3	N/A	N/A
	40 mm/s	Time	5.628 s	N/A	N/A
		Length	206.322 mm	N/A	N/A
		Volume	530.437 mm^3	N/A	N/A
Swiping	10 mm/s	Time	47.604 s	N/A	N/A
		Length	459.242 mm	N/A	N/A
		Volume	4486.661 mm^3	N/A	N/A
	40 mm/s	Time	12.036 s	N/A	N/A
		Length	411.509 mm	N/A	N/A
		Volume	1134.389 mm^3	N/A	N/A

Table A2 (Appendix). Same as Table A1, but for the large OR (43×86 mm^2).

Strategy	Nominal speed	Measured parameter	With *arc ON* over the whole toolpath	With *arc OFF* outside the OR	
				Over the whole toolpath	When *arc* is *ON*
Raster-pass	10 mm/s	Time	N/A	167.436 s	87.708 s
		Length	N/A	1636.161 mm	860.635 mm
		Volume	N/A	8270.973 mm^3	8265.319 mm^3
	40 mm/s	Time	N/A	44.880 s	23.436 s
		Length	N/A	1634.200 mm	859;632 mm
		Volume	N/A	2220.143 mm^3	2206.573 mm^3
Triangular 45°	10 mm/s	Time	96.612 s	100.368 s	87.084 s
		Length	959.644 mm	961.592 mm	861.657 mm
		Volume	9105.649 mm^3	8346.780 mm^3	8204.245 mm^3
	40 mm/s	Time	24.312 s	28.128 s	22.812 s
		Length	939.284 mm	941.410 mm	860.906 mm
		Volume	2291.398 mm^3	2220.143 mm^3	2151.154 mm^3
Triangular 60°	10 mm/s	Time	94.140 s	97.932 s	87.096 s
		Length	936.174 mm	938.188 mm	861.729 mm
		Volume	8872.663 mm^3	8376.156 mm^3	8204.245 mm^3
	40 mm/s	Time	23.712 s	27.600s	22.824 s
		Length	917.451 mm	922.234 mm	862.392 mm
		Volume	2234.848 mm^3	2226.929 mm^3	2148.892 mm^3
Triangular 90°	10 mm/s	Time	91.800 s	95.616 s	87.036 s
		Length	914.583 mm	916.983 mm	861.650 mm
		Volume	8652.119 mm^3	8336.571 mm^3	8199.721 mm^3
	40 mm/s	Time	23.124 s	26.988 s	22.956 s
		Length	895.988 mm	907.158 mm	861.719 mm
		Volume	2179.429 mm^3	2226.929 mm^3	2160.202 mm^3
Rectangular	10 mm/s	Time	87.360 s	N/A	N/A
		Length	869.174 mm	N/A	N/A
		Volume	8233.651 mm^3	N/A	N/A
	40 mm/s	Time	21.996 s	N/A	N/A
		Length	848.838 mm	N/A	N/A
		Volume	2073.116 mm^3	N/A	N/A
Semi-circular	10 mm/s	Time	92.304 s	96.024 s	87.228 s
		Length	921.243 mm	922.426 mm	861.216 mm
		Volume	8699.621 mm^3	8277.759 mm^3	8221.210 mm^3
	40 mm/s	Time	23.232 s	27.060 s	23.244 s
		Length	901.752 mm	911.362 mm	860.474 mm
		Volume	2189.68 mm^3	2206.571 mm^3	2188.477 mm^3
Spiral	10 mm/s	Time	87.192 s	N/A	N/A
		Length	867.889 mm	N/A	N/A
		Volume	8217.817 mm^3	N/A	N/A
	40 mm/s	Time	21.936 s	N/A	N/A
		Length	847.85 mm	N/A	N/A
		Volume	2067.461 mm^3	N/A	N/A
Swiping	10 mm/s	Time	185.652 s	N/A	N/A
		Length	1831.387 mm	N/A	N/A
		Volume	17497.639 mm^3	N/A	N/A
	40 mm/s	Time	46.596 s	N/A	N/A
		Length	1730.3393 mm	N/A	N/A
		Volume	4391.657 mm^3	N/A	N/A

Table A3 (Appendix). Impact of switching between *arc ON* and *arc OFF* for the four strategies featuring a toolpath outside the OR. Comparison is made for two nominal speeds and two OR areas (21.5×43 mm^2 and 43×86 mm^2, simply written "small" and "large" respectively in the table).

Strategy	Nominal speed	OR size	Total time	With *arc OFF* outside the OR	With *arc ON* over the whole toolpath
Semi-circular	10 mm/s	Small	inside the OR	22.524 s	21.552 s
			outside the OR	3.612 s	2.832 s
		Large	inside the O.R	87.708 s	86.184 s
			outside the OR	8.316 s	6.12 s
	40 mm/s	Small	inside the OR	6.372 s	5.628 s
			outside the OR	1.536 s	0.636 s
		Large	inside the OR	23.604 s	21.852 s
			outside the OR	3.444 s	1.380 s
Triangular 45°	10 mm/s	Small	inside the OR	22.152 s	21.660 s
			outside the OR	1.644 s	4.620 s
		Large	inside the OR	87.456 s	86.160 s
			outside the OR	12.912 s	10.452 s
	40 mm/s	Small	inside the OR	6.288 s	5.580 s
			outside the OR	1.644 s	1.152 s
		Large	inside the OR	23.172 s	21.720 s
			outside the OR	4.956 s	2.592 s
Triangular 60°	10 mm/s	Small	inside the OR	22.152 s	21.684 s
			outside the OR	4.524 s	3.528 s
		Large	inside the OR	87.468 s	86.124 s
			outside the OR	10.308 s	8.016 s
	40 mm/s	Small	inside the OR	6.216 s	5.580 s
			outside the OR	1.956 s	0.876 s
		Large	inside the OR	23.208 s	21.708 s
			outside the OR	4.392 s	2.004 s
Triangular 90°	10 mm/s	Small	inside the OR	22.332 s	21.648 s
			outside the OR	3.516 s	2.508 s
		Large	inside the OR	87.552 s	86.196 s
			outside the OR	8.064 s	5.604 s
	40 mm/s	Small	inside the OR	6.288 s	5.664 s
			outside the OR	1.644 s	0.516 s
		Large	inside the OR	23.316 s	21.840 s
			outside the OR	3.672 s	1.284 s